atoms

MDPI

Article

Parametric Calculations of Radiative Decay Rates for Magnetic Dipole and Electric Quadrupole Transitions in Tm IV, Yb V, and Er IV

Wan-Ü Lydia Tchang-Brillet [1,*], Jean-François Wyart [1,2], Ali Meftah [1,3] and Sofiane Ait Mammar [3,4]

1 LERMA, Observatoire de Paris-Meudon, PSL Research University, CNRS UMR8112, Sorbonne Université, F-92195 Meudon, France; jean-francois.wyart@u-psud.fr (J.-F.W.); ali.meftah@obspm.fr (A.M.)
2 Laboratoire Aimé Cotton, CNRS UMR9188, Univ Paris-Sud, ENS Cachan, Univ Paris-Saclay, bâtiment 505, F-91405 Orsay CEDEX, France
3 Laboratoire de Physique et Chimie Quantique, Université Mouloud Mammeri, BP 17 RP, 15000 Tizi-Ouzou, Algeria; sofiane.aitmammar@yahoo.ca
4 Université d'Alger 1—Benyoucef Benkhedda, 2 Rue Didouche Mourad, Alger 16000, Algeria
* Correspondence: lydia.tchang-brillet@obspm.fr

Received: 18 August 2018; Accepted: 9 September 2018; Published: 12 September 2018

Abstract: Semi-empirical transition probabilities for magnetic dipole (M1) and electric quadrupole (E2) emission lines have been derived from parametric studies of experimental energy levels in Tm^{3+} (Tm IV), Yb^{4+} (Yb V), and Er^{3+} (Er IV), using Cowan codes. Results are compared with those existing from ab initio calculations or from more sophisticated semi-empirical calculations. Satisfactory agreements show that simple parametric calculations can provide good predictions on line intensities, provided that experimental levels are available, allowing reliable fits of energy parameters.

Keywords: atomic spectra; transition probabilities; lanthanide ions; parametric calculations

1. Introduction

The radiative properties of lanthanide ions have since long attracted interest because of the numerous applications of these ions in solid-state laser materials, photonics, or the lighting industry (see [1] and references therein for example). Radiative transitions were observed in doped crystals or in solution with small displacements relative to free ions, and their interpretation was helped by the knowledge of free ion structures and transition probabilities [2,3]. In astrophysics, Hubble Space Telescope observations of spectra of chemically peculiar stars show the presence of lanthanide ions up to doubly charged stages (see [4] for example). More recently, simultaneously observed emissions of electromagnetic waves and gravitational waves during two neutron stars merging increased the interest for radiative properties of higher charged lanthanide ions [5,6].

Due to the presence of 4f open shell electrons, lanthanide ions have very complex spectra, which can be untangled only by high-resolution laboratory studies. Systematic comparison of variation trends in energy parameters along isoelectronic or isoionic sequences is also a necessary help. During the past years, our collaborating team has carried out analyses of high-resolution spectra of several lanthanide ions in the vacuum ultra-violet (VUV) region [7–14], which contains essentially the fourth and fifth spectra and partially the third spectra. Experimental spectra were produced using high-voltage vacuum spark sources. Their interpretations in terms of atomic structures were supported by parametric calculations of energies and transition probabilities using the COWAN program package RCN/RCN2/RCG/RCE [15] in its Windows version [16]. As the analysis makes progress and experimental level energies become known, an iterative least-squares fit of energy parameters, i.e., the radial integrals, is performed in the RCE code, minimizing the differences between

the calculated and the experimental energy values. In all of our previous works, this semi-empirical approach was shown to provide constantly improved predictions for unknown energy levels, and for observed intensities of spectral lines.

In the plasma of vacuum sparks, observed emitted lines are electric dipole (E1) transitions, the electron density being too high (around 10^{18} cm^{-3}) for the observation of forbidden transitions such as magnetic dipole (M1) or electric quadrupole (E2) transitions. However, these transitions become observable in low density astrophysical or laboratory plasmas. It is therefore worth the effort to obtain good predictions for them. Early in the 1960s, Carnall et al. [2,3] already investigated spectral intensities within the ground-state $4f^n$ configurations of the trivalent lanthanides in solution, in relation to theoretical calculations of transition probabilities by Judd [17] and Ofelt [18]. Recently, Dodson and Zia [19] reported ab initio calculations of emission rates and oscillator strengths for the M1 and E2 transitions in triply ionized lanthanide ions (Ce IV–Yb IV). The authors of [19] used a detailed free ion Hamiltonian, including electrostatic and spin-orbit terms as well as two-body, three-body, spin-spin, spin-other-orbit, and electrostatically correlated spin-orbit interactions. Semi-empirical calculations are possible when experimental level energies are available. Enzonga Yoca and Quinet [20] introduced the experimental level energies from Meftah et al. [11] into semi-empirical calculations for Tm IV, and reported the radiative decay rates for E1, M1, and E2 transitions obtained by the pseudo-relativistic Hartree-Fock (HFR) approach, including configuration interactions and core-polarization effects. Li et al. [21] reported semi-empirical radiative rates for M1 and E2 transitions of Ba-like ions within the $4f^2$ configuration, and also of Yb V within the $4f^{12}$ configuration. The authors fitted the experimental energy levels from Meftah et al. [12] to a standard f-shell Hamiltonian, including not only the major electrostatic and spin-orbit terms, but also various minor contributions like two-body, spin-spin, and spin-other orbit terms [21].

The main purpose of our present work is to explore the reliability of semi-empirical forbidden (M1 and E2) transition probabilities that we may derive from our spectral analyses of allowed transitions in a rather simple way by using Cowan codes; in particular, for the recently analyzed Er IV spectrum. Furthermore, the results are compared with ab initio results by Dodson and Zia [19]. The cases of Tm IV and Yb V are also studied for a comparison of our results to the previous results obtained by more sophisticated semi-empirical methods respectively, in Enzonga Yoca and Quinet [20] and Li et al. [21].

2. Experimental and Theoretical Methods

The present semi-empirical calculations were based on experimental level energies resulting from high-resolution studies of high voltage vacuum spark emission spectra recorded on the 10 m vacuum spectrograph of the Meudon Observatory (3600 lines/mm holographic concave grating, linear dispersion 0.25 Å/mm in the focal plane, resolution 0.008 Å in a wavelength range of 200–3000 Å). The overall uncertainty on the measured wavelengths varied between $\pm$ 0.003 and 0.005 Å. Analyses of these spectra with the resolution of fine structures, based on the Ritz combination principle, led to the determination of energy levels of the studied ion. The energy values of the levels were optimized by the least-squares fit, minimizing differences between the experimental wavenumbers and the calculated (Ritz) wavenumbers [22]. The uncertainty on the experimental energies could be estimated as $\pm$ 0.3–1 cm^{-1} in most cases. More experimental details can be found in previous publications (see Ref [12] for example).

The parametric calculations supporting the analyses are based on the standard Central Field Approximation and the Perturbation Theory. The Hamiltonian can be written as: $H = H_0 + H_1$, where H_0 is the zero-order central field Hamiltonian and $H_1 = Q + \Lambda$, the perturbation Hamiltonian, with the terms of the electrostatic interactions Q and the terms of the spin-orbit interactions Λ. The calculations were performed using the COWAN program package RCN/RCN2/RCG/RCE. A first step consisted of Hartree-Fock calculations of radial integrals, including relativistic corrections (HFR) performed by running RCN and RCN2. In this step, atomic orbitals and average energies of configurations E_{Av} were optimized. Then, the Hamiltonian matrix was diagonalized in RCG, leading to energy

values and eigenvectors of levels in intermediate coupling. The diagonalization took place in a basis, generally in a LS-coupling scheme, including the close configurations of a given parity, which possibly undergo mutual configuration interactions (CI). Each matrix element of H_1 was written as a sum of products: $H_{1ij} = \sum_{\alpha} c_{ij}^{\alpha} P_{\alpha}$, where c_{ij}^{α} are angular coefficients that are derived from angular momentum algebra and P_{α} are radial integrals, which are also designated as energy parameters. Explicit configuration interactions are described by off-diagonal matrix elements between interacting configurations. Two-body electrostatic interactions from far configurations are taken into account by the introduction of effective parameters. When experimental energies are available, RCE is run for iterative least-squares fits minimizing the differences between the calculated and experimental energies, where the radial integrals are used as fitted parameters. The mean error of the fit is defined by $\Delta E = \sqrt{\sum_{i} \left(E_i^{exp} - E_i^{calc}\right)^2 / (N_i - N_p)}$, where N_i is the number of known experimental energies and N_p is the number of free parameters. To avoid too large a number of free parameters, some constraints on parameters could be introduced by fixing their values or by fixing their ratios to their HFR values. After convergence, the final parameters were used in a final diagonalization, providing the best predictions for unknown energy levels. The corresponding level compositions in the intermediate coupling scheme are used for the calculations of the Landé factors and the radiative transition probabilities, log gf (g: statistical weight of the lower level, f: the absorption oscillator strength) and gA (g: statistical weight of the upper level, A: the Einstein spontaneous emission coefficient). These quantities are thus semi-empirical values based on experimental energies, and they hopefully represent better predictions than ab initio ones. The consistency between the observed intensities and calculated gA values for electric dipole transitions was also a criterion for the reliability of transition identifications. The RCG code output displayed a cancellation factor (CF), along with the gA value of a spectral line, which is defined by Equation (14.107), p. 432 in [15]. The CF is an indication of possible destructive interference effects in line strength calculations involving amplitudes in wavefunctions with intermediate-coupling and configuration–interaction mixings. According to Cowan [15], "Computed line strengths may be expected to show large percent errors when CF is smaller than about 0.1 or 0.05". However, this limit seems to be rather restrictive, since in the case of Dy I quoted by Cowan [15], a good correlation between the observed intensities and the computed gf values for CF of greater than about 0.02 was found.

With the final fitted energy parameters, the Cowan programs could be run for calculations of magnetic dipole (M1) and electric quadrupole (E2) transition probabilities with specific options involving the matrix elements of the corresponding operators. We carried out these calculations for three lanthanide ions for which we have experimental energies derived from our previous analyses, i.e., Tm^{3+} (Tm IV) [11], Yb^{4+} (Yb V) [12], and Er^{3+} (Er IV) [14]. The reliability of our results was checked by comparison with available results from other calculations, either ab initio or semi-empirical. In the following, the results of Tm IV were compared with ab initio results by Dodson and Zia [19] and semi-empirical ones from Enzonga Yoca and Quinet [20]. Results on Yb V were compared with semi-empirical ones from Li et al. [21]. For Er IV, the present work reported the first semi-empirical results and compared them with ab initio ones by Dodson and Zia [19].

In each case, the comparison was carried out on the one hand, for the values of transition rate gA, and on the other hand, for the line strengths S, so to eliminate the wavelength dependences. Indeed, in different codes, the primary calculated quantity for each transition was the line strength. Transition rate is proportional to the line strength, with a factor varying over $(\lambda)^{-3}$ for a M1 emission line, and over $(\lambda)^{-5}$ for an E2 emission line [15]. A consistent comparison between the different calculations should involve line strengths. It is also possible to scale the gA values to the experimental wavelengths. The Ritz wavelengths derived from fitted energies (λ_{Ritz_Fit}) were rather close to the ones that were derived from experimental energies (λ_{Ritz_Exp}), but this was not the case for ab initio calculated wavelengths (λ_{calc}). The numerical factors of conversion between gA (s^{-1}) and S (a.u.), with λ in angström, can be found in the NIST Atomic Spectra Database [23]:

$$\text{M1 lines: } S = 3.707342 \times 10^{-14}\ \lambda^3\ gA;$$

$$\text{E2 line: } S = 8.928970 \times 10^{-19}\ \lambda^5\ gA.$$

3. Results and Discussion

3.1. Tm IV

The Tm IV case is a favorable one to commence comparisons. The analysis of the Tm^{3+} free ion spectrum [11] in the 700–2320 Å range resulted in the determination of 10 levels of the ground-state configuration $4f^{12}$, together with 9, 33, and 157 levels of, respectively, the $4f^{11}6s$, $4f^{11}6p$, and $4f^{11}5d$-excited configurations. The parametric interpretation of the configurations reported in [11] involved a basis of three even configurations $5p^64f^{12}$, $5p^64f^{11}6p$, and $5p^54f^{13}$, and a basis of three odd configurations $5p^64f^{11}5d$, $5p^64f^{11}6s$, and $5p^54f^{12}5d$. Progress was made [24] since the last publication, with one more experimental level in the ground-state configuration $4f^{12}$ (^{3}P J = 1), localized at E = 36,763.8 cm^{-1}. Thus a new parametric calculation was performed in the present work, including as well a fourth even configuration $5p^54f^{12}6p$ into the basis allowing calculations of gA values for the M1 and E2 transition with the new set of parameters. Table 1 reports the final parameter values of the fit for the even parity levels of $5p^64f^{12}$ and $5p^64f^{11}6p$ configurations, although they are only slightly different from the set reported in Table 5 of [11]. The set of electrostatic (F^k, G^k) and spin-orbit parameters (ζ) was completed by effective parameters α, β, and γ related to two-body excitation in f^n subshells, and by "illegal" Slater parameters F^1(f,p) and G^3(f,p) acting on the (S, L) terms of the f^np configurations, which drastically improve the calculated energies. The perturbing configurations $5p^54f^{13}$ and $5p^54f^{12}6p$ were experimentally unknown. They were introduced in the basis set with all relevant parameters (scaled HFR) and $E_{av}(5p^54f^{13})$ = 235,589 cm^{-1}, and $E_{av}(5p^54f^{12}6p)$ = 361,860 cm^{-1} fixed. All the configuration interaction parameters R^k were fixed to their HFR values. The corresponding mean error of the fit was 46 cm^{-1}.

Table 2 shows the comparison between different calculations of the M1 and E2 transition probabilities. Following the presentation of [20] where the authors listed the transition probabilities gA that were greater than 0.01 s^{-1} for M1 and E2 decays within the $4f^{12}$ ground-state configuration, and compared them to the ab initio calculations by Dodson and Zia [19], we listed the corresponding results from the present work. The first column displays the predicted Ritz wavelengths λ_{Ritz_Exp} of the M1 and E2 lines derived from experimental level energies [11]. All the gA values (col. 5–7) have been converted into line strengths S (col. 8–10) using the wavelengths involved in the corresponding calculations, i.e., the ab initio calculated wavelengths for conversion of ab initio gA values [19] (col. 6) and Ritz wavelengths derived from our fitted energies for conversion of our gA values (col. 7). The corresponding wavelengths are respectively listed in col. 11 and col. 12 of Table 2. As for the gA values of Enzonga Yoca and Quinet (col. 5) [20], we used the λ_{Ritz_Exp} for conversion in the absence of indications on the authors' wavelengths. This is reasonable, since, as already mentioned, λ_{Ritz_Fit} were very close to λ_{Ritz_Exp}, and the factors $(\lambda_{Ritz\_fit}/\lambda_{Ritz\_exp})^3$ or $(\lambda_{Ritz\_fit}/\lambda_{Ritz\_Exp})^5$ would produce changes of less than 3%.

Figure 1 shows the distribution of M1 and E2 line strengths of Table 2 versus experimental wavelengths for Tm IV. One can see that for M1 transitions, our parametric calculations led to results that are in good agreement with the semi-empirical calculations in [20], and with the ab initio calculations in [19]. The standard deviation is about 2% between our results and the previous semi-empirical results [20], and is about 9% between our results and the ab initio results [19]. The predicted line at 4266 Å, a mixture of M1 and E2, had a M1 line strength showing a large discrepancy with the ab initio value [19]. The corresponding gA value was not explicitly given in [20]. For this line, the cancellation factor (CF) derived in our calculations from Cowan codes was 0.00, meaning an unreliable result. For E2, the three calculations give more scattered results. However, for the lines at 3039, 3847, 4437, 4721, 5759, 6402 and 7968 Å, indicated in [20] as having large discrepancies with ab initio values, our values are much closer to the values in [20]. One may note that in Tm

IV, the E2 transitions have line strengths of two orders of magnitude lower than the M1 transitions. The cancellation factors calculated in this work were on average smaller for E2 than for the M1, meaning that the gA values are less reliable for E2 transitions.

Table 1. Parameter values (in cm^{-1}) for $4f^{12}$ and $4f^{11}6p$ in Tm IV from a least-squares fit including four even configurations. Experimental energy values are from [11,24]. The perturbing configurations $5p^54f^{13}$ and $5p^54f^{12}6p$ are introduced in the basis set with all relevant parameters (scaled HFR), and $E_{av}(5p^54f^{13})$ = 235,589 cm^{-1} and $E_{av}(5p^54f^{12}6p)$ = 361,860 cm^{-1} fixed. The constrained parameters are indicated in the columns "St. Dev" by 'r' (linked by a constant ratio) and by 'f' (fixed).

Param.	Fitted	St. Dev.	HF	Scaling	Fitted	St. Dev.	HF	Scaling
	$4f^{12}$				$4f^{11}6p$			
Eav	18,193	16			191,160	28		
F^2(ff)	104,222	187	132,844	0.785	109,640	197	139,572	0.786
F^4(ff)	72,149	313	73,322	0.866	77,203	335	87,892	0.878
F^6(ff)	51,056	393	59,937	0.852	55,404	427	53,328	0.875
α	21	1			21	1		
β	−905	52			−905	52		
γ	1991	r			1991	r		
ζ_f	2640	6	2688	0.982	2796	6	2843	0.983
ζ_p					5567	13	4758	1.170
F^1(fp)					296	54		
F^2(fp)					7995	205	9357	0.854
G^2(fp)					2331	67	2399	0.972
G^3(fp)					0	f		
G^4(fp)					1917	67	2173	0.882
R^2(ff,fp)	−3599	f	−3599	1.00				
R^2(ff,fp)	−1910	f	−1910	1.00				

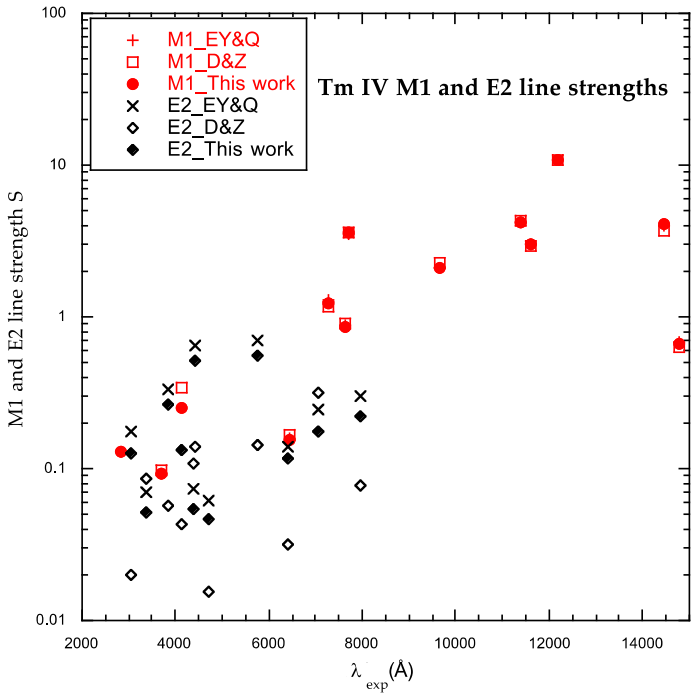

Figure 1. Magnetic dipole (M1) and electric quadrupole (E2) line strengths in Tm IV for lines between 2000 and 15,000 Å.

Table 2. Transition probabilities gA (s^{-1}) and line strengths for magnetic dipole (M1) and electric quadrupole (E2) transitions within the Tm IV ground-state configuration $4f^{12}$. Comparison with existing results. All wavelengths are in vacuum.

Transitions [a]				gA (s^{-1})			Line Strength S (a.u.)			Wavelengths (Å)	
λ_{Ritz_Exp} (Å)	Lower E (cm^{-1})	Upper E (cm^{-1})	Type	EY&Q [20]	D&Z [19]	This Work	EY&Q [b]	D&Z [c]	This Work	$\lambda_{D\&Z}$	λ_{Ritz_Fit}
2830.511	0.00 (6)	35,329.31 (6)	M1	1.52×10^{2}		1.52×10^{2}	1.28×10^{-1}		1.28×10^{-1}		2831.3
3039.658	5634.02 (4)	38,532.46 (2)	E2	7.51×10^{-1}	7.50×10^{-2}	5.37×10^{-1}	1.74×10^{-1}	2.01×10^{-2}	1.26×10^{-1}	3130	3048.6
3367.537	5634.02 (4)	35,329.31 (6)	E2	1.83×10^{-1}	1.95×10^{-1}	1.31×10^{-1}	7.08×10^{-2}	8.63×10^{-2}	5.12×10^{-2}	3460	3374.2
3688.325	8216.73 (5)	35,329.31 (6)	M1	4.94×10^{1}	4.56×10^{1}	4.94×10^{1}	9.19×10^{-2}	9.65×10^{-2}	9.18×10^{-2}	3850	3690.1
3848.340	12,547.23 (4)	38,532.46 (2)	E2	4.47×10^{-1}	5.95×10^{-2}	3.44×10^{-1}	3.37×10^{-1}	5.65×10^{-2}	2.64×10^{-1}	4030	3862.6
4145.585	14,410.41 (3)	38,532.46 (2)	M1 E2	9.10×10^{1}	1.15×10^{2} 3.25×10^{-2}	9.51×10^{1} 1.18×10^{-1}	2.40×10^{-1}	3.38×10^{-1} 4.27×10^{-2}	2.51×10^{-1} 1.34×10^{-1}	4300	4171.8
4265.691	15,089.60 (2)	38,532.46 (2)	M1 E2	1.32×10^{-1}	1.78 1.08×10^{-3}	3.00×10^{-1} 2.78×10^{-3}	3.80×10^{-4}	5.75×10^{-3} 1.65×10^{-3}	8.63×10^{-4} 3.57×10^{-3}	4430	4280.1
4389.415	12,547.23 (4)	35,329.31 (6)	E2	5.05×10^{-2}	5.99×10^{-2}	3.64×10^{-2}	7.35×10^{-2}	1.08×10^{-1}	5.36×10^{-2}	4580	4400.6
4438.678	5634.02 (4)	28,163.25 (2)	E2	4.24×10^{-1}	7.50×10^{-2}	3.38×10^{-1}	6.52×10^{-1}	1.38×10^{-1}	5.20×10^{-1}	4600	4438.6
4722.729	0.00 (6)	21,174.20 (4)	E2	2.94×10^{-2}	6.93×10^{-3}	2.21×10^{-2}	6.17×10^{-2}	1.53×10^{-2}	4.60×10^{-2}	4770	4715.9
5760.946	21,174.20 (4)	38,532.46 (2)	E2	1.22×10^{-1}	1.81×10^{-2}	9.49×10^{-2}	6.91×10^{-1}	1.42×10^{-1}	5.50×10^{-1}	6150	5787.0
6403.680	12,547.23 (4)	28,163.25 (2)	E2	1.45×10^{-2}	2.39×10^{-3}	1.21×10^{-2}	1.39×10^{-1}	3.18×10^{-2}	1.16×10^{-1}	6830	6403.2
6434.932	5634.02 (4)	21,174.20 (4)	M1	1.59×10^{1}	1.72×10^{1}	1.58×10^{1}	1.57×10^{-1}	1.66×10^{-1}	1.56×10^{-1}	6390	6442.5
7064.587	21,174.20 (4)	35,329.31 (6)	E2	1.55×10^{-2}	1.46×10^{-2}	1.10×10^{-2}	2.44×10^{-1}	3.19×10^{-1}	1.75×10^{-1}	7550	7084.7
7271.225	14,410.41 (3)	28,163.25 (2)	M1	8.99×10^{1}	7.00×10^{1}	8.73×10^{1}	1.28	1.16	1.24	7650	7300.2
7648.973	15,089.60 (2)	28,163.25 (2)	M1	5.26×10^{1}	4.65×10^{1}	5.21×10^{1}	8.73×10^{-1}	9.08×10^{-1}	8.64×10^{-1}	8080	7638.6
7717.556	8216.73 (5)	21,174.20 (4)	M1	2.08×10^{2}	2.04×10^{2}	2.09×10^{2}	3.54	3.64	3.56	7840	7701.4
7969.887	0.00 (6)	12,547.23 (4)	E2	1.05×10^{-2}	2.54×10^{-3}	7.93×10^{-3}	3.01×10^{-1}	7.76×10^{-2}	2.23×10^{-1}	8070	7939.6
9643.936	28,163.25 (2)	38,532.46 (2)	M1	6.33×10^{1}	6.50×10^{1}	6.33×10^{1}	2.10	2.29	2.10	9830	9734.8
11,394.21	5634.02 (4)	14,410.41 (3)	M1	7.68×10^{1}	7.62×10^{1}	7.73×10^{1}	4.21	4.35	4.24	11,550	11,323
11,591.56	12,547.23 (4)	21,174.20 (4)	M1	5.26×10^{1}	5.04×10^{1}	5.28×10^{1}	3.04	2.97	3.05	11,670	11,615
12,170.29	0.00 (6)	8216.73 (5)	M1	1.61×10^{2}	1.60×10^{2}	1.62×10^{2}	1.08×10^{1}	1.07×10^{1}	1.08×10^{1}	12,190	12,166
14,465.06	5634.02 (4)	12,547.23 (4)	M1	3.56×10^{1}	3.56×10^{1}	3.68×10^{1}	3.99	3.72	4.13	14,120	14,467
14,784.61	14,410.41 (3)	21,174.20 (4)	M1	5.64	5.84	5.59	6.76×10^{-1}	6.35×10^{-1}	6.69×10^{-1}	14,310	14,946
23,092.02	8216.73 (5)	12,547.23 (4)	M1	1.43×10^{1}		1.45×10^{1}	6.53		6.61		22,857
38,719.02	5634.02 (4)	8216.73 (5)	M1	4.09×10^{-1}		4.02×10^{-1}	8.80×10^{-1}		8.64×10^{-1}		39,414
53,671.68	12,547.23 (4)	14,410.41 (3)	M1	3.42×10^{-1}		3.67×10^{-1}	1.96		2.10		52,112

[a] λ_{Ritz_Exp} (col. 1) calculated from experimental energies (col. 2 and 3) from [11]; [b] line strength calculated using gA from EY&Q [20] and λ_{Ritz_Exp} (Å) of col. 1; [c] line strength calculated using gA and $\lambda_{D\&Z}$ from Dodson and Zia [19].

3.2. Yb V

The analysis of the Yb V spectrum, isoelectronic to Tm IV, was achieved by Meftah et al. [12] with the determination of all 13 energy levels of the ground-state configuration $4f^{12}$, and respectively, 174, 12, and 43 levels of the excited configurations $4f^{11}5d$, 6s, and 6p. The parametric study of the even parity included $4f^{12}$, $4f^{11}6p$, and the unknown core-excited configurations $5p^54f^{13}$ and $5p^54f^{12}6p$. The least-squares fit minimizing the differences between calculated and experimental energies involved 56 even parity levels and resulted in a mean error of 55 cm^{-1}. In the present work, using the final fitted values of parameters reported in Table 5 of [12], we calculated the transition probabilities gA for the forbidden M1 and E2 transitions within the ground-sate configuration $4f^{12}$ of Yb V, and compared them in Table 3 with the results from semi-empirical calculations by Li et al. [21]. We also converted gA to line strengths S, as described above. The cancellation factors are listed in the last column, and all but three values are smaller than 0.02.

Figure 2 displays the M1 and E2 line strengths in Yb V in the wavelength range reduced to 2000–8000 Å for clarity. One can see that the two sets of line strengths are in good agreement, with relative differences less than 3% for M1 lines, except for 3810 Å and 28,836 Å, and less than 10% for E2 lines, except for the lines et 2702, 3810, and 4133 Å. It can be noticed in Table 3 that each of these transitions involved one level with a strong mixing of LS components. Indeed, for the levels 6112.03 cm^{-1} (4), 24,192.89 cm^{-1} (4), and 43,119.5 cm^{-1} (2), Meftah et al [12] reported the main LS components with the percentage compositions of 62% ^{1}G, 56% ^{3}H, and 56% ^{1}D ($4f^{12}$), respectively. The calculated gA could be rather sensitive to small changes in these percentages.

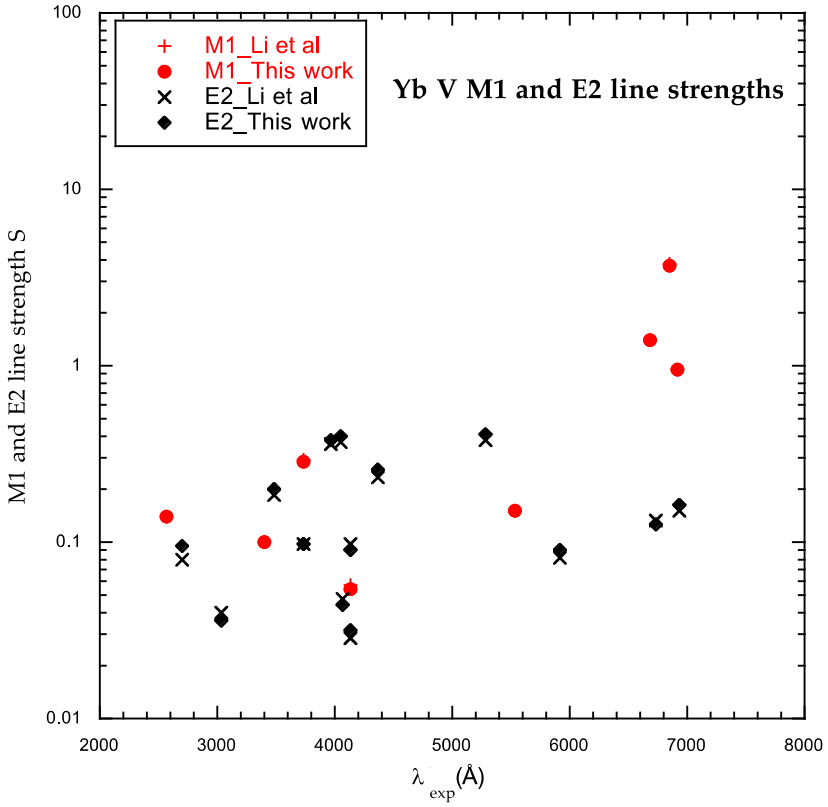

Figure 2. Magnetic dipole (M1) and electric quadrupole (E2) line strengths in Yb V for lines between 2000 and 8000 Å.

Table 3. Transition probabilities gA (s^{-1}) and line strengths for magnetic dipole (M1) and electric quadrupole (E2) transitions within the Yb V ground-state configuration $4f^{12}$. Comparison with existing results (ordered by increasing upper level energies). All wavelengths are in vacuum. CF is the cancellation factor as defined by Equation (14.107), p. 432 in [15], and derived from our calculations.

Transitions [a]				gA (s^{-1})		Line Strength S (a.u.)		Wavelength		CF
λ_{Ritz_Exp} (Å)	Lower E (cm^{-1})	Upper E (cm^{-1})	Type	Li et al. [21]	This Work	Li et al. [b]	This Work	$\lambda_{Li\ et\ al.}$ (Å)	λ_{Ritz_Fit} (Å)	This Work
2702.157	6112.03 (4)	43,119.5 (2)	E2	6.25×10^{-1}	7.37×10^{-1}	8.01×10^{-2}	9.48×10^{-2}	2700	2707.74	−0.13
3482.561	14,405.00 (4)	43,119.5 (2)	E2	4.02×10^{-1}	4.38×10^{-1}	1.83×10^{-1}	2.00×10^{-1}	3480	3485.58	−0.48
3738.694	16,372.19 (3)	43,119.5 (2)	M1 E2	1.52×10^{2} 1.50×10^{-1}	1.47×10^{2} 1.48×10^{-1}	2.95×10^{-1} 9.80×10^{-2}	2.86×10^{-1} 9.70×10^{-2}	3740	3743.51	−1.00 −0.64
3810.656	16,877.3 (2)	43,119.5 (2)	M1 E2	2.08×10^{-1} 3.50×10^{-3}	1.37×10^{-1} 2.79×10^{-3}	4.28×10^{-4} 2.51×10^{-3}	2.79×10^{-4} 1.99×10^{-3}	3810	3805.28	0.00 −0.01
5283.566	24,192.89 (4)	43,119.5 (2)	E2	1.03×10^{-1}	1.07×10^{-1}	3.79×10^{-1}	4.09×10^{-1}	5280	5320.84	0.94
8474.720	31,319.7 (2)	43,119.5 (2)	M1	9.92×10^{1}	9.66×10^{1}	2.23	2.22	8470	8520.91	0.05
49,053.27	41,080.9 (1)	43,119.5 (2)	M1	3.29×10^{-1}	3.70×10^{-1}	1.44	1.47	49,060	47,524.2	1.00
4047.156	16,372.19 (3)	41,080.9 (1)	E2	3.78×10^{-1}	4.05×10^{-1}	3.68×10^{-1}	4.01×10^{-1}	4050	4063.60	−0.98
4131.617	16,877.3 (2)	41,080.9 (1)	M1 E2	2.16×10^{1} 9.00×10^{-2}	2.09×10^{1} 8.33×10^{-2}	5.64×10^{-2} 9.66×10^{-2}	5.48×10^{-2} 9.01×10^{-2}	4130	4136.49	−1.00 −0.39
10,244.64	31,319.7 (2)	41,080.9 (1)	M1	2.55×10^{1}	2.37×10^{1}	1.01	9.84×10^{-1}	10,240	10,382.4	1.00
77,555.45	39,791.5 (0)	41,080.9 (1)	M1	1.09×10^{-1}	8.78×10^{-2}	1.88	1.88	77,540	83,340.9	1.00
4364.106	16,877.3 (2)	39,791.5 (0)	E2	1.66×10^{-1}	1.83×10^{-1}	2.34×10^{-1}	2.55×10^{-1}	4360	4352.52	−0.96
2561.613	0.00 (6)	39,037.9 (6)	M1	2.24×10^{2}	2.26×10^{2}	1.39×10^{-1}	1.41×10^{-1}	2560	2558.31	−0.01
3037.126	6112.03 (4)	39,037.9 (6)	E2	1.70×10^{-1}	1.53×10^{-1}	3.95×10^{-2}	3.57×10^{-2}	3040	3042.98	−0.29
3394.662	9579.89 (5)	39,037.9 (6)	M1	6.94×10^{1}	7.04×10^{1}	1.00×10^{-1}	1.01×10^{-1}	3390	3386.90	−1.00
4059.611	14,405.00 (4)	39,037.9 (6)	E2	4.80×10^{-2}	4.45×10^{-2}	4.72×10^{-2}	4.40×10^{-2}	4060	4061.58	0.77
6736.270	24,192.89 (4)	39,037.9 (6)	E2	1.06×10^{-2}	9.71×10^{-3}	1.32×10^{-1}	1.25×10^{-1}	6740	6791.00	−0.71
3967.047	6112.03 (4)	31,319.7 (2)	E2	4.12×10^{-1}	4.36×10^{-1}	3.62×10^{-1}	3.83×10^{-1}	3970	3968.98	−0.58
5912.017	14,405.00 (4)	31,319.7 (2)	E2	1.27×10^{-2}	1.41×10^{-2}	8.21×10^{-2}	8.96×10^{-2}	5910	5898.40	−0.18
6690.077	16,372.19 (3)	31,319.7 (2)	M1	1.25×10^{2}	1.27×10^{2}	1.38	1.40	6690	6676.88	1.00

Table 3. *Cont.*

Transitions [a]				gA (s^{-1})		Line Strength S (a.u.)		Wavelength		CF
λ_{Ritz_Exp} (Å)	Lower E (cm^{-1})	Upper E (cm^{-1})	Type	Li et al. [21]	This Work	Li et al. [b]	This Work	$\lambda_{Li\ et\ al.}$ (Å)	λ_{Ritz_Fit} (Å)	This Work
6924.057	16,877.3 (2)	31,319.7 (2)	M1	7.83×10^{1}	7.93×10^{1}	9.61×10^{-1}	9.56×10^{-1}	6920	6875.94	−0.06
4133.446	0.00 (6)	24,192.89 (4)	E2	2.67×10^{-2}	3.07×10^{-2}	2.87×10^{-2}	3.19×10^{-2}	4130	4104.59	0.34
5530.710	6112.03 (4)	24,192.89 (4)	M1	2.38×10^{1}	2.42×10^{1}	1.49×10^{-1}	1.50×10^{-1}	5530	5513.54	0.00
6843.222	9579.89 (5)	24,192.89 (4)	M1	3.22×10^{2}	3.26×10^{2}	3.82	3.73	6840	6756.70	1.00
10,216.71	14,405.00 (4)	24,192.89 (4)	M1	7.79×10^{1}	8.06×10^{1}	3.08	3.08	10,220	10,105.5	−0.02
12,786.58	16,372.19 (3)	24,192.89 (4)	M1	8.35	8.86	6.48×10^{-1}	6.62×10^{-1}	12,790	12,628.1	−1.00
9289.131	6112.03 (4)	16,877.3 (2)	E2	3.27×10^{-3}	3.38×10^{-3}	2.02×10^{-1}	2.20×10^{-1}	9290	9387.99	0.90
197,976.7	16,372.19 (3)	16,877.3 (2)	M1	1.75×10^{-2}	1.10×10^{-2}	5.03	5.01	197,710	230,631	1.00
9746.437	6112.03 (4)	16,372.19 (3)	M1	1.24×10^{2}	1.21×10^{2}	4.25	4.21	9750	9786.35	1.00
50,833.93	14,405.00 (4)	16,372.19 (3)	M1	3.85×10^{-1}	3.97×10^{-1}	1.89	1.90	50,930	50,589.0	1.00
6942.034	0.00 (6)	14,405.00 (4)	E2	1.06×10^{-2}	1.16×10^{-2}	1.53×10^{-1}	1.63×10^{-1}	6940	6912.09	−0.76
12,058.41	6112.03 (4)	14,405.00 (4)	M1	5.91×10^{1}	5.89×10^{1}	3.84	3.90	12,050	12,133.6	0.03
20,724.92	9579.89 (5)	14,405.00 (4)	M1	1.89×10^{1}	2.00×10^{1}	6.21	6.28	20,700	20,389.2	1.00
10,438.53	0.00 (6)	9579.89 (5)	M1	2.56×10^{2}	2.54×10^{2}	1.08×10^{1}	1.08×10^{1}	10,440	10,457.1	1.00
28,836.23	6112.03 (4)	9579.89 (5)	M1	9.09×10^{-1}	8.46×10^{-1}	8.09×10^{-1}	8.44×10^{-1}	28,850	29,966.6	−1.00

[a] λ_{Ritz_Exp} (col. 1) calculated from experimental energies (col. 2 and 3) from [12]; [b] line strength is calculated using gA and $\lambda_{Li\ et\ al.}$ from Li et al. [21].

3.3. Er IV

The recent analysis [14] of Er IV, isoionic of Tm IV, led to the determination of 120 energy levels belonging to the lower parts of the four configurations $4f^{11}$, $4f^{10}5d$, 6s, and 6p. Unfortunately, the experimental energies of the $4f^{11}$ ground-state configuration that comprises 41 levels were less completely known than in Tm IV and Yb V cases. However, in the parametric study of the odd-parity configurations, the least-squares fit with 11 free parameters upon respectively nine and 29 known levels of $4f^{11}$ and $4f^{10}6p$ resulted in a mean error of 41 cm^{-1}, which was quite satisfactory for the average energies of respectively $E_{av}(4f^{11})$ = 35,997 cm^{-1} and $E_{av}(4f^{10}6p)$ = 207,022 cm^{-1}. Using the parameters of the final fit given in Table 4 of [14], we calculated the semi-empirical transition probabilities for M1 and E2 transitions within the ground-state configuration $4f^{11}$ of Er IV. Table 4 reports the present results on M1 transitions between 3000 Å and 17,000 Å, the ab initio values of which are available in Dodson and Zia [19] to make a comparison possible. Table 5 reports similar results for E2 transition probabilities. Figure 3a,b display respectively the M1 and E2 line strengths from the present work versus the ab initio results from [19].

The large number of spectral lines in Er IV encourages an examination of possible correlation between discrepancies with ab initio results and cancellation factors (CF). These are listed in the last columns of Tables 4 and 5. Figure 3a shows that the M1 line strengths are in good agreement. Most of the M1 line strengths have a relative discrepancy of less than 5%, except for the eight lines. Three of them (4623, 5868, 6016 Å) have a CF of 0.00, four others (2975, 3660, 4094, 10,328 Å) have CF between 0.02 and 0.04, and one (13,752 Å) has a CF of 0.08. For the E2 transitions, the results are more scattered, with 90 in 113 lines showing discrepancies of less than 15%. Three lines (4608, 5233, and 14,568 Å) have been discarded on the figure since their line strengths differ by one or two orders of magnitude. Discrepancies are also more or less correlated to cancellation factors without an absolute rule. In the absence of CF values from the ab initio calculations [19], the CF values listed in Tables 4 and 5 only characterize the present results and they do not fully explain the discrepancies observed.

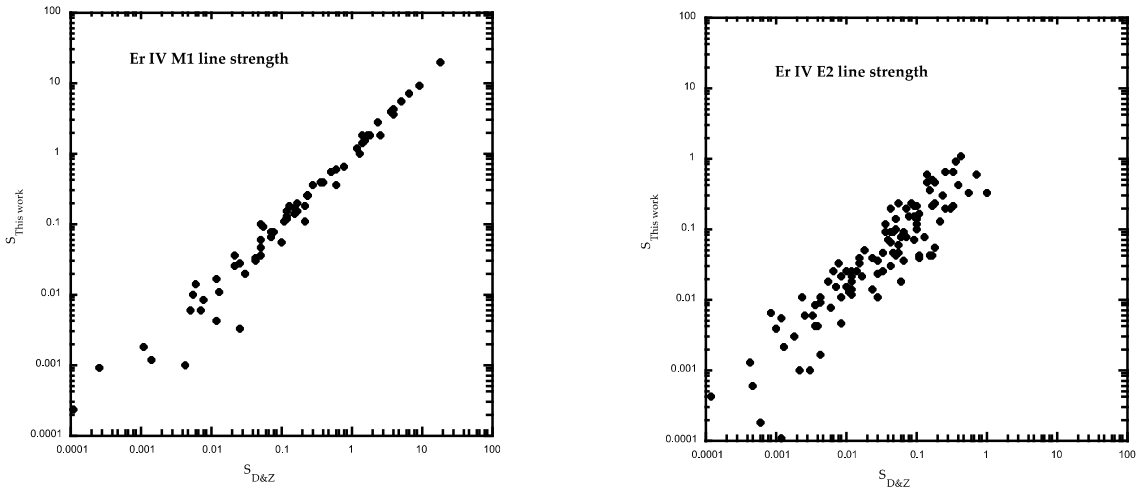

(**a**) (**b**)

Figure 3. (**a**) Magnetic dipole (M1) and (**b**) electric quadrupole (E2) line strengths in Er IV for the lines between 2000 and 17,000 Å (Cf. Tables 4 and 5).

Table 4. Semi-empirical transition probabilities gA (s^{-1}) and line strengths for magnetic dipole (M1) transitions within the Er IV ground-state configuration $4f^{11}$. Comparison with ab initio results from Dodson and Zia [19]. All wavelengths are in vacuum. Each energy level is specified by its energy value, followed by the quantum number J between parentheses [14]. CF is the cancellation factor as defined by Equation (14.107), p. 432 in [15] and derived from our calculations.

Transition [a]						gA (s^{-1})		Line Strength S (a.u.)		Wavelength	CF
E_{Low_Fit} (cm^{-1})	E_{Upp_Fit} (cm^{-1})	λ_{Ritz_Fit} (Å)	E_{Low_Exp} (cm^{-1})	E_{Upp_Exp} (cm^{-1})	λ_{Ritz_Exp} (Å)	This Work	D&Z [19]	This Work	D&Z [19]	$\lambda_{D\&Z}$ (Å) [19]	This Work
−32 (7.5)	33,577.5 (6.5)	2975.36	0.00			1.38×10^{1}	5.64	1.34×10^{-2}	6.05×10^{-3}	3070	−0.02
−32 (7.5)	28,232.5 (7.5)	3538.04	0.00			3.17×10^{2}	2.91×10^{2}	5.21×10^{-1}	5.29×10^{-1}	3660	0.00
12,399.5 (4.5)	39,716.6 (3.5)	3660.64	12,468.66			1.23×10^{-1}	4.91×10^{-2}	2.24×10^{-4}	1.11×10^{-4}	3940	0.04
6533.4 (6.5)	33,577.5 (6.5)	3697.69	6507.75			7.48×10^{1}	7.35×10^{1}	1.40×10^{-1}	1.54×10^{-1}	3840	0.01
10,184.6 (5.5)	36,928.1 (4.5)	3739.18	10,171.79			5.82×10^{1}	5.34×10^{1}	1.13×10^{-1}	1.19×10^{-1}	3920	−0.05
12,399.5 (4.5)	36,928.1 (4.5)	4076.83	12,468.66			1.04×10^{1}	9.20	2.62×10^{-2}	2.58×10^{-2}	4230	0.00
15,295.1 (4.5)	39,716.6 (3.5)	4094.71	15,404.86			3.38×10^{-1}	8.16×10^{-2}	8.59×10^{-4}	2.58×10^{-4}	4400	0.03
10,184.6 (5.5)	33,577.5 (6.5)	4274.85	10,171.79			5.26×10^{1}	5.26×10^{1}	1.52×10^{-1}	1.73×10^{-1}	4460	1.00
12,399.5 (4.5)	34,405.9 (3.5)	4544.05	12,468.66			2.11×10^{1}	1.94×10^{1}	7.33×10^{-2}	7.89×10^{-2}	4790	0.14
6533.4 (6.5)	28,232.5 (7.5)	4608.54	6507.75			6.94×10^{1}	6.05×10^{1}	2.52×10^{-1}	2.50×10^{-1}	4810	0.27
15,295.1 (4.5)	36,928.1 (4.5)	4622.57	15,404.86			2.64	1.36	9.68×10^{-3}	5.47×10^{-3}	4770	0.00
18,470.4 (1.5)	39,201.1 (2.5)	4823.77				1.54×10^{1}	1.36×10^{1}	6.41×10^{-2}	7.10×10^{-2}	5200	0.43
6533.4 (6.5)	26,807.1 (5.5)	4932.41	6507.75	26,707.79	4950.485	1.39×10^{2}	1.49×10^{2}	6.26×10^{-1}	8.17×10^{-1}	5290	0.99
20,527.2 (3.5)	39,716.6 (3.5)	5211.17				2.12×10^{-1}	2.18×10^{-1}	1.11×10^{-3}	1.46×10^{-3}	5660	0.00
15,295.1 (4.5)	34,405.9 (3.5)	5232.61	15,404.86			5.84	7.26	3.10×10^{-2}	4.48×10^{-2}	5500	−0.02
20,527.2 (3.5)	39,201.1 (2.5)	5355.02				1.91×10^{1}	3.03×10^{1}	1.09×10^{-1}	2.23×10^{-1}	5830	0.79
10,184.6 (5.5)	27,798.8 (4.5)	5677.15	10,171.79	27,766.82	5683.423	2.73	3.52	1.86×10^{-2}	3.05×10^{-2}	6160	−0.01
22,159.1 (2.5)	39,716.6 (3.5)	5695.56				8.14	5.62	5.58×10^{-2}	5.16×10^{-2}	6280	0.66
19,385.4 (5.5)	36,928.1 (4.5)	5700.34	19,331.69			4.86×10^{1}	3.96×10^{1}	3.34×10^{-1}	2.92×10^{-1}	5840	0.07
22,159.1 (2.5)	39,201.1 (2.5)	5867.83				5.37×10^{-1}	1.21	4.02×10^{-3}	1.22×10^{-2}	6490	0.00
22,533.3 (1.5)	39,201.1 (2.5)	5999.59				1.99	1.15	1.60×10^{-2}	1.22×10^{-2}	6600	−0.04
10,184.6 (5.5)	26,807.1 (5.5)	6015.86	10,171.79	26,707.79	6047.412	1.17×10^{-1}	4.28×10^{-1}	9.59×10^{-4}	4.44×10^{-3}	6540	0.00
18,470.4 (1.5)	34,889.8 (2.5)	6090.38				1.51×10^{-4}	3.27×10^{-2}	1.26×10^{-6}	2.62×10^{-4}	6000	0.00
20,527.2 (3.5)	36,928.1 (4.5)	6097.28				8.61	7.67	7.23×10^{-2}	7.08×10^{-2}	6290	0.08
12,399.5 (4.5)	28,265.1 (3.5)	6302.82	12,468.66			1.31×10^{1}	1.16×10^{1}	1.22×10^{-1}	1.28×10^{-1}	6670	−0.19
12,399.5 (4.5)	27,798.8 (4.5)	6493.70	12,468.66	27,766.82	6536.731	1.63×10^{1}	1.04×10^{1}	1.69×10^{-1}	1.31×10^{-1}	6970	0.01

Table 4. *Cont.*

Transition [a]						gA (s^{-1})		Line Strength S (a.u.)		Wavelength	CF
E_{Low_Fit} (cm^{-1})	E_{Upp_Fit} (cm^{-1})	λ_{Ritz_Fit} (Å)	E_{Low_Exp} (cm^{-1})	E_{Upp_Exp} (cm^{-1})	λ_{Ritz_Exp} (Å)	This Work	D&Z [19]	This Work	D&Z [19]	$\lambda_{D\&Z}$ (Å) [19]	This Work
18,470.4 (1.5)	33,755.8 (2.5)	6542.31				5.48×10^{-1}	4.16×10^{-1}	5.69×10^{-3}	5.09×10^{-3}	6910	1.00
18,470.4 (1.5)	33,598.6 (0.5)	6610.17				2.38×10^{1}	2.26×10^{1}	2.54×10^{-1}	2.50×10^{-1}	6680	−1.00
24,723.5 (4.5)	39,716.6 (3.5)	6669.61	24,736.00			3.95	3.74	4.34×10^{-2}	5.47×10^{-2}	7330	1.00
10,184.6 (5.5)	24,723.5 (4.5)	6877.96	10,171.79	24,736.00	6866.147	9.57×10^{1}	8.48×10^{1}	1.15	1.24	7330	0.31
12,399.5 (4.5)	26,807.1 (5.5)	6940.69	12,468.66	26,707.79	7022.901	2.78	3.48	3.56×10^{-2}	5.38×10^{-2}	7470	−0.03
20,527.2 (3.5)	34,889.8 (2.5)	6962.46				1.38×10^{2}	1.20×10^{2}	1.72	1.44	6860	0.99
19,385.4 (5.5)	33,577.5 (6.5)	7046.41	19,331.69			7.99×10^{-1}	9.76×10^{-1}	1.04×10^{-2}	1.31×10^{-2}	7120	−0.29
20,527.2 (3.5)	34,405.9 (3.5)	7205.30				2.71×10^{1}	2.52×10^{1}	3.76×10^{-1}	4.12×10^{-1}	7610	−0.02
18,470.4 (1.5)	31,890.1 (1.5)	7451.74				2.43×10^{1}	2.22×10^{1}	3.73×10^{-1}	3.67×10^{-1}	7640	−0.02
20,527.2 (3.5)	33,755.8 (2.5)	7559.41				1.75	2.35	2.81×10^{-2}	4.57×10^{-2}	8070	−0.51
15,295.1 (4.5)	28,265.1 (3.5)	7710.08	15,404.86			5.02	2.80	8.54×10^{-2}	5.58×10^{-2}	8130	−0.06
6533.4 (6.5)	19,385.4 (5.5)	7780.69	6507.75	19,331.69	7797.916	2.18×10^{2}	1.79×10^{2}	3.83	3.82	8320	−0.99
22,159.1 (2.5)	34,889.8 (2.5)	7854.99				1.08×10^{1}	1.00×10^{1}	1.94×10^{-1}	1.76×10^{-1}	7800	−0.01
15,295.1 (4.5)	27,798.8 (4.5)	7997.65	15,404.86	27,766.82	8089.332	1.81×10^{1}	2.58×10^{1}	3.56×10^{-1}	6.04×10^{-1}	8580	−0.02
22,533.3 (1.5)	34,889.8 (2.5)	8092.91				7.65	6.66	1.50×10^{-1}	1.24×10^{-1}	7950	0.07
12,399.5 (4.5)	24,723.5 (4.5)	8114.08	12,468.66	24,736.00	8151.727	1.94	1.39×10^{-2}	3.90×10^{-2}	3.16×10^{-4}	8500	0.00
22,159.1 (2.5)	34,405.9 (3.5)	8165.47				8.88	8.64	1.79×10^{-1}	2.17×10^{-1}	8780	−0.43
24,723.5 (4.5)	36,928.1 (4.5)	8193.62	24,736.00			1.29×10^{2}	1.12×10^{2}	2.63	2.49	8430	0.01
27,798.8 (4.5)	39,716.6 (3.5)	8390.60	27,766.82			7.50	6.00	1.64×10^{-1}	1.64×10^{-1}	9040	1.00
22,159.1 (2.5)	33,755.8 (2.5)	8623.26				1.43	7.14×10^{-1}	3.40×10^{-2}	2.20×10^{-2}	9400	−0.04
15,295.1 (4.5)	26,807.1 (5.5)	8686.64	15,404.86	26,707.79	8847.264	1.00×10^{1}	8.41	2.57×10^{-1}	2.53×10^{-1}	9330	−0.45
28,265.1 (3.5)	39,716.6 (3.5)	8732.30				5.52	4.98	1.36×10^{-1}	1.63×10^{-1}	9600	−0.02
22,533.3 (1.5)	33,755.8 (2.5)	8910.83				9.25×10^{-1}	6.54×10^{-1}	2.43×10^{-2}	2.16×10^{-2}	9620	−0.97
22,533.3 (1.5)	33,598.6 (0.5)	9037.21				2.08×10^{-1}	2.66×10^{-1}	5.71×10^{-3}	7.68×10^{-3}	9200	0.91
28,265.1 (3.5)	39,201.1 (2.5)	9143.89				3.66	3.04	1.04×10^{-1}	1.17×10^{-1}	10,110	−0.38
26,807.1 (5.5)	36,928.1 (4.5)	9880.38	26,707.79			1.18×10^{2}	1.19×10^{2}	4.21	4.13	9780	−1.00
22,159.1 (2.5)	31,890.1 (1.5)	10,276.4				3.57×10^{1}	3.28×10^{1}	1.43	1.53	10,810	−0.49
24,723.5 (4.5)	34,405.9 (3.5)	10,327.9	24,736.00			2.46	1.06	1.00×10^{-1}	5.22×10^{-2}	10,980	−0.03
15,295.1 (4.5)	24,723.5 (4.5)	10,606.3	15,404.86	24,736.00	10,716.80	1.18×10^{2}	1.04×10^{2}	5.37	5.15	11,010	0.02

Table 4. *Cont.*

Transition [a]						gA (s^{-1})		Line Strength S (a.u.)		Wavelength	CF
E_{Low_Fit} (cm^{-1})	E_{Upp_Fit} (cm^{-1})	λ_{Ritz_Fit} (Å)	E_{Low_Exp} (cm^{-1})	E_{Upp_Exp} (cm^{-1})	λ_{Ritz_Exp} (Å)	This Work	D&Z [19]	This Work	D&Z [19]	$\lambda_{D\&Z}$ (Å) [19]	This Work
22,533.3 (1.5)	31,890.1 (1.5)	10,687.4				3.93×10^{1}	3.42×10^{1}	1.78	1.74	11,110	0.28
10,184.6 (5.5)	19,385.4 (5.5)	10,868.4	10,171.79	19,331.69	10,917.15	2.84×10^{1}	2.34×10^{1}	1.35	1.47	11,920	0.01
27,798.8 (4.5)	36,928.1 (4.5)	10,953.7	27,766.82			3.61×10^{1}	4.11×10^{1}	1.76	1.90	10,770	−0.02
28,265.1 (3.5)	36,928.1 (4.5)	11,543.4				1.42×10^{-1}	1.41×10^{-1}	8.11×10^{-3}	8.10×10^{-3}	11,570	0.00
19,385.4 (5.5)	27,798.8 (4.5)	11,885.7	19,331.69	27,766.82	11,855.18	1.37×10^{2}	1.22×10^{2}	8.53	9.40	12,760	1.00
12,399.5 (4.5)	20,527.2 (3.5)	12,303.0	12,468.66			2.63×10^{1}	3.17×10^{1}	1.82	2.54	12,940	1.00
20,527.2 (3.5)	28,265.1 (3.5)	12,923.6				7.27	6.14	5.82×10^{-1}	5.96×10^{-1}	13,780	0.02
19,385.4 (5.5)	26,807.1 (5.5)	13,473.9	19,331.69	26,707.79	13,557.30	3.99×10^{1}	3.43×10^{1}	3.62	3.89	14,510	0.01
31,890.1 (1.5)	39,201.1 (2.5)	13,678.1				1.04×10^{1}	8.46	9.83×10^{-1}	1.35	16,270	−1.00
20,527.2 (3.5)	27,798.8 (4.5)	13,752.4		27,766.82		3.38×10^{-2}	2.00×10^{-1}	3.26×10^{-3}	2.56×10^{-2}	15,120	−0.08
12,399.5 (4.5)	19,385.4 (5.5)	14,314.2	12,468.66	19,331.69	14,570.82	2.35	1.76	2.55×10^{-1}	2.37×10^{-1}	15,370	−0.06
26,807.1 (5.5)	33,577.5 (2.5)	14,771.3	26,707.79			1.46×10^{-2}	1.12×10^{-2}	1.74×10^{-3}	1.13×10^{-3}	13,990	0.30
28,265.1 (3.5)	34,889.8 (2.5)	15,094.5				4.03×10^{-1}	1.11	5.14×10^{-2}	1.05×10^{-1}	13,670	0.29
27,798.8 (4.5)	34,405.9 (3.5)	15,134.9	27,766.82			5.46×10^{1}	5.14×10^{1}	7.02	6.87	15,330	0.89
−32 (7.5)	6533.4 (6.5)	15,231.3	0.00	6507.75	15,366.29	1.44×10^{2}	1.43×10^{2}	1.89×10^{1}	1.89×10^{1}	15,280	1.00

[a] λ_{Ritz_Fit} (col. 3) and λ_{Ritz_Exp} (col. 6) are respectively calculated from least-squares fitted energies (col. 1 and 2) and experimental energies (col. 4 and 5) in [14].

Table 5. Semi-empirical transition probabilities gA (s^{-1}) and line strengths for electric quadrupole (E2) transitions within the Er IV ground-state configuration $4f^{11}$. Comparison with ab initio results from Dodson and Zia [19]. All wavelengths are in vacuum. Each energy level is specified by its energy value, followed by the quantum number J between the parentheses [14]. CF is the cancellation factor as defined by Equation (14.107), p. 432 in [15] and derived from our calculations.

Transition [a]						gA (s^{-1})		Line Strength S (a.u.)		Wavelength (Å)	CF
E_{Low_Fit} (cm^{-1})	E_{Upp_Fit} (cm^{-1})	λ_{Ritz_Fit} (Å)	E_{Low_Exp} (cm^{-1})	E_{Upp_Exp} (cm^{-1})	λ_{Ritz_Exp} (Å)	This Work	D&Z [19]	This Work	D&Z [19]	$\lambda_{D\&Z}$ [19]	This Work
−32.0 (7.5)	33,577.5 (6.5)	2975.36	0.00			1.40×10^{-2}	7.63×10^{-3}	2.91×10^{-3}	1.86×10^{-3}	3070	−0.51
6533.4 (6.5)	36,928.1 (4.5)	3290.00	6507.75			4.03×10^{-1}	1.19×10^{-1}	1.39×10^{-1}	5.04×10^{-2}	3430	−0.58
10,184.6 (5.5)	39,716.6 (3.5)	3386.09	10,171.79			2.68×10^{-2}	7.32×10^{-3}	1.06×10^{-2}	4.29×10^{-3}	3660	−0.10
−32.0 (7.5)	28,232.5 (7.5)	3538.04	0.00			4.09×10^{-2}	2.96×10^{-2}	2.02×10^{-2}	1.74×10^{-2}	3660	0.23
12,399.5 (4.5)	39,716.6 (3.5)	3660.64	12,468.66			1.51×10^{-1}	7.72×10^{-2}	8.87×10^{-2}	6.54×10^{-2}	3940	−0.40
6533.4 (6.5)	33,577.5 (6.5)	3697.69	6507.75			6.99×10^{-3}	5.38×10^{-3}	4.31×10^{-3}	4.01×10^{-3}	3840	0.21
−32.0 (7.5)	26,807.1 (5.5)	3725.85	0.00	26,707.79	3744.226	1.37	4.39×10^{-1}	8.82×10^{-1}	3.68×10^{-1}	3930	0.75
12,399.5 (4.5)	39,201.1 (2.5)	3731.04	12,468.66			7.37×10^{-2}	1.96×10^{-2}	4.76×10^{-2}	1.84×10^{-2}	4020	0.22
10,184.6 (5.5)	36,928.1 (4.5)	3739.18	10,171.79			1.30×10^{-2}	4.56×10^{-3}	8.46×10^{-3}	3.77×10^{-3}	3920	−0.04
12,399.5 (4.5)	36,928.1 (4.5)	4076.83	12,468.66			4.18×10^{-3}	3.07×10^{-3}	4.21×10^{-3}	3.71×10^{-3}	4230	0.01
15,295.1 (4.5)	39,716.6 (3.5)	4094.71	15,404.86			3.26×10^{-1}	1.07×10^{-1}	3.35×10^{-1}	1.58×10^{-1}	4400	−0.57
10,184.6 (5.5)	34,405.9 (3.5)	4128.53	10,171.79			4.71×10^{-1}	1.17×10^{-1}	5.04×10^{-1}	1.72×10^{-1}	4400	0.77
15,295.1 (4.5)	39,201.1 (2.5)	4183.00	15,404.86			1.95×10^{-1}	3.48×10^{-2}	2.23×10^{-1}	5.80×10^{-2}	4510	0.74
10,184.6 (5.5)	33,577.5 (6.5)	4274.85	10,171.79			7.81×10^{-4}	1.36×10^{-3}	9.95×10^{-4}	2.15×10^{-3}	4460	−0.05
12,399.5 (4.5)	34,889.8 (2.5)	4446.25	12,468.66			1.37×10^{-2}	5.21×10^{-3}	2.13×10^{-2}	8.39×10^{-3}	4480	−0.20
12,399.5 (4.5)	34,405.9 (3.5)	4544.05	12,468.66			1.43×10^{-2}	4.61×10^{-3}	2.48×10^{-2}	1.04×10^{-2}	4790	0.06
6533.4 (6.5)	28,232.5 (7.5)	4608.54	6507.75			7.31×10^{-5}	1.33×10^{-6}	1.36×10^{-4}	3.06×10^{-6}	4810	0.03
15,295.1 (4.5)	36,928.1 (4.5)	4622.57	15,404.86			3.19×10^{-3}	1.22×10^{-3}	6.02×10^{-3}	2.69×10^{-3}	4770	0.02
12,399.5 (4.5)	33,755.8 (2.5)	4682.38				2.78×10^{-1}	5.45×10^{-2}	5.59×10^{-1}	1.48×10^{-1}	4970	0.78
6533.4 (6.5)	27,798.8 (4.5)	4702.38	6507.75	27,766.82	4703.875	5.01×10^{-1}	1.49×10^{-1}	1.03	4.33×10^{-1}	5040	0.97
18,470.4 (1.5)	39,716.6 (3.5)	4706.74				1.56×10^{-1}	3.60×10^{-1}	3.21×10^{-1}	1.07	5060	0.83
12,399.5 (4.5)	33,577.5 (6.5)	4721.95	12,468.66			1.41×10^{-2}	1.83×10^{-2}	2.96×10^{-2}	4.49×10^{-2}	4870	−0.08
18,470.4 (1.5)	39,201.1 (2.5)	4823.77				8.65×10^{-2}	1.03×10^{-1}	2.02×10^{-1}	3.50×10^{-1}	5200	0.43
19,385.4 (5.5)	39,716.6 (3.5)	4918.45	19,331.69			2.45×10^{-1}	6.90×10^{-2}	6.29×10^{-1}	2.55×10^{-1}	5290	−0.89
6533.4 (6.5)	26,807.1 (5.5)	4932.41	6507.75	26,707.79	4950.485	3.69×10^{-2}	1.42×10^{-2}	9.62×10^{-2}	5.24×10^{-2}	5290	0.93
15,295.1 (4.5)	34,889.8 (2.5)	5103.35	15,404.86			1.06×10^{-2}	5.14×10^{-3}	3.26×10^{-2}	1.58×10^{-2}	5100	−0.20
−32.0 (7.5)	19,385.4 (5.5)	5149.93	0.00	19,331.69	5172.853	2.01×10^{-1}	8.74×10^{-2}	6.51×10^{-1}	3.55×10^{-1}	5390	0.90

Table 5. *Cont.*

Transition [a]						gA (s^{-1})		Line Strength S (a.u.)		Wavelength (Å)	CF
E_{Low_Fit} (cm^{-1})	E_{Upp_Fit} (cm^{-1})	λ_{Ritz_Fit} (Å)	E_{Low_Exp} (cm^{-1})	E_{Upp_Exp} (cm^{-1})	λ_{Ritz_Exp} (Å)	This Work	D&Z [19]	This Work	D&Z [19]	$\lambda_{D\&Z}$ [19]	This Work
20,527.2 (3.5)	39,716.6 (3.5)	5211.17				6.67×10^{-2}	3.77×10^{-2}	2.29×10^{-1}	1.95×10^{-1}	5660	−0.69
15,295.1 (4.5)	34,405.9 (3.5)	5232.61	15,404.86			3.10×10^{-5}	3.06×10^{-7}	1.09×10^{-4}	1.37×10^{-6}	5500	0.00
20,527.2 (3.5)	39,201.1 (2.5)	5355.02				2.26×10^{-2}	6.30×10^{-3}	8.87×10^{-2}	3.79×10^{-2}	5830	−0.35
15,295.1 (4.5)	33,755.8 (2.5)	5416.89	15,404.86			5.47×10^{-2}	1.59×10^{-2}	2.28×10^{-1}	8.85×10^{-2}	5740	−0.68
15,295.1 (4.5)	33,577.5 (6.5)	5469.92	15,404.86			2.16×10^{-4}	6.23×10^{-4}	9.43×10^{-4}	3.06×10^{-3}	5600	0.02
6533.4 (6.5)	24,723.5 (4.5)	5497.37	6507.750	24,736.00	5485.990	1.46×10^{-2}	7.45×10^{-3}	6.53×10^{-2}	4.33×10^{-2}	5790	0.55
10,184.6 (5.5)	28,265.1 (3.5)	5530.72	10,171.79			1.00×10^{-1}	2.86×10^{-2}	4.62×10^{-1}	1.87×10^{-1}	5930	0.71
10,184.6 (5.5)	28,232.5 (7.5)	5540.93	10,171.79			9.58×10^{-3}	9.46×10^{-3}	4.47×10^{-2}	5.69×10^{-2}	5830	−0.23
10,184.6 (5.5)	27,798.8 (4.5)	5677.15	10,171.79	27,766.82	5683.423	1.63×10^{-2}	5.82×10^{-3}	8.59×10^{-2}	4.61×10^{-2}	6160	0.58
22,159.1 (2.5)	39,716.6 (3.5)	5695.56				7.66×10^{-3}	6.22×10^{-3}	4.10×10^{-2}	5.43×10^{-2}	6280	0.29
19,385.4 (5.5)	36,928.1 (4.5)	5700.34	19,331.69			3.33×10^{-3}	9.38×10^{-4}	1.79×10^{-2}	5.69×10^{-3}	5840	0.05
22,533.3 (1.5)	39,716.6 (3.5)	5819.61				8.89×10^{-3}	1.95×10^{-2}	5.30×10^{-2}	1.84×10^{-1}	6380	0.40
22,159.1 (2.5)	39,201.1 (2.5)	5867.83				2.70×10^{-2}	1.13×10^{-2}	1.68×10^{-1}	1.17×10^{-1}	6490	−0.39
22,533.3 (1.5)	39,201.1 (2.5)	5999.59				1.83×10^{-2}	1.96×10^{-2}	1.27×10^{-1}	2.19×10^{-1}	6600	0.47
10,184.6 (5.5)	26,807.1 (5.5)	6015.86	10,171.79	26,707.79	6047.412	2.57×10^{-5}	5.68×10^{-5}	1.81×10^{-4}	6.06×10^{-4}	6540	−0.01
18,470.4 (1.5)	34,889.8 (2.5)	6090.38				5.22×10^{-3}	1.69×10^{-2}	3.91×10^{-2}	1.17×10^{-1}	6000	−0.14
20,527.2 (3.5)	36,928.1 (4.5)	6097.28				6.10×10^{-3}	5.55×10^{-3}	4.59×10^{-2}	4.88×10^{-2}	6290	0.11
18,470.4 (1.5)	34,405.9 (3.5)	6275.39				1.22×10^{-3}	2.55×10^{-3}	1.06×10^{-2}	2.79×10^{-2}	6570	−0.26
12,399.5 (4.5)	28,265.1 (3.5)	6302.82	12,468.66			1.70×10^{-2}	7.02×10^{-3}	1.51×10^{-1}	8.28×10^{-2}	6670	0.27
12,399.5 (4.5)	27,798.8 (4.5)	6493.70	12,468.66	27,766.82	6536.734	4.47×10^{-4}	6.06×10^{-4}	4.61×10^{-3}	8.90×10^{-3}	6970	−0.03
18,470.4 (1.5)	33,755.8 (2.5)	6542.31				3.35×10^{-3}	4.96×10^{-3}	3.59×10^{-2}	6.97×10^{-2}	6910	0.42
18,470.4 (1.5)	33,598.6 (0.5)	6610.17				4.93×10^{-4}	1.04×10^{-4}	5.56×10^{-3}	1.24×10^{-3}	6680	0.09
19,385.4 (5.5)	34,405.9 (3.5)	6657.47	19,331.69			4.10×10^{-3}	1.28×10^{-3}	4.79×10^{-2}	1.87×10^{-2}	6960	−0.17
24,723.5 (4.5)	39,716.6 (3.5)	6669.61	24,736.00			1.31×10^{-2}	5.17×10^{-3}	1.54×10^{-1}	9.76×10^{-2}	7330	−0.30
22,159.1 (2.5)	36,928.1 (4.5)	6771.04				1.11×10^{-3}	1.59×10^{-3}	1.41×10^{-2}	2.51×10^{-2}	7070	0.00
10,184.6 (5.5)	24,723.5 (4.5)	6877.96	10,171.79	24,736.00	6866.147	2.85×10^{-3}	1.27×10^{-3}	3.91×10^{-2}	2.40×10^{-2}	7330	0.20
24,723.5 (4.5)	39,201.1 (2.5)	6907.07	24,736.00			8.30×10^{-3}	1.63×10^{-3}	1.17×10^{-1}	3.75×10^{-2}	7630	−0.21
12,399.5 (4.5)	26,807.1 (5.5)	6940.69	12,468.66	26,707.79	7022.901	4.70×10^{-3}	4.78×10^{-3}	6.76×10^{-2}	9.92×10^{-2}	7470	−0.17
20,527.2 (3.5)	34,889.8 (2.5)	6962.46				8.65×10^{-4}	8.34×10^{-4}	1.26×10^{-2}	1.13×10^{-2}	6860	0.08

Table 5. *Cont.*

Transition [a]						gA (s^{-1})		Line Strength S (a.u.)		Wavelength (Å)	CF
E_{Low_Fit} (cm^{-1})	E_{Upp_Fit} (cm^{-1})	λ_{Ritz_Fit} (Å)	E_{Low_Exp} (cm^{-1})	E_{Upp_Exp} (cm^{-1})	λ_{Ritz_Exp} (Å)	This Work	D&Z [19]	This Work	D&Z [19]	$\lambda_{D\&Z}$ [19]	This Work
19,385.4 (5.5)	33,577.5 (6.5)	7046.41	19,331.69			4.89×10^{-4}	3.85×10^{-4}	7.58×10^{-3}	6.29×10^{-3}	7120	−0.18
20,527.2 (3.5)	34,405.9 (3.5)	7205.30				7.70×10^{-3}	4.40×10^{-3}	1.34×10^{-1}	1.00×10^{-1}	7610	−0.34
18,470.4 (1.5)	31,890.1 (1.5)	7451.74				3.57×10^{-3}	3.04×10^{-3}	7.32×10^{-2}	7.06×10^{-2}	7640	−0.56
20,527.2 (3.5)	33,755.8 (2.5)	7559.41				1.72×10^{-3}	5.39×10^{-4}	3.80×10^{-2}	1.65×10^{-2}	8070	0.43
15,295.1 (4.5)	28,265.1 (3.5)	7710.08	15,404.86			4.46×10^{-6}	3.86×10^{-5}	1.09×10^{-4}	1.23×10^{-3}	8130	0.00
26,807.1 (5.5)	39,716.6 (3.5)	7746.03	26,707.79			1.79×10^{-2}	4.07×10^{-3}	4.45×10^{-1}	1.46×10^{-1}	8330	−0.44
6533.4 (6.5)	19,385.4 (5.5)	7780.69	6507.75	19,331.69	7797.915	8.13×10^{-4}	4.75×10^{-4}	2.07×10^{-2}	1.69×10^{-2}	8320	0.26
22,159.1 (2.5)	34,889.8 (2.5)	7854.99				2.12×10^{-3}	2.21×10^{-3}	5.66×10^{-2}	5.71×10^{-2}	7800	0.18
15,295.1 (4.5)	27,798.8 (4.5)	7997.65	15,404.86	27,766.82	8089.332	7.08×10^{-3}	4.12×10^{-3}	2.07×10^{-1}	1.71×10^{-1}	8580	−0.83
22533.3 (1.5)	34,889.8 (2.5)	8092.90				5.45×10^{-4}	2.14×10^{-3}	1.69×10^{-2}	6.06×10^{-2}	7950	−0.10
12,399.5 (4.5)	24,723.5 (4.5)	8114.08	12,468.66	24,736.00	8151.726	4.36×10^{-4}	3.06×10^{-4}	1.37×10^{-2}	1.21×10^{-2}	8500	−0.04
22,159.1 (2.5)	34,405.9 (3.5)	8165.47				6.03×10^{-3}	5.70×10^{-3}	1.96×10^{-1}	2.65×10^{-1}	8780	−0.43
24,723.5 (4.5)	36,928.1 (4.5)	8193.62	24,736.00			2.34×10^{-3}	1.60×10^{-3}	7.73×10^{-2}	6.08×10^{-2}	8430	0.14
27,798.8 (4.5)	39,716.6 (3.5)	8390.60	27,766.82			5.54×10^{-3}	1.86×10^{-3}	2.06×10^{-1}	1.00×10^{-1}	9040	−0.85
22,533.3 (1.5)	34,405.9 (3.5)	8422.87				1.13×10^{-3}	2.26×10^{-3}	4.30×10^{-2}	1.17×10^{-1}	8970	0.30
22159.1 (2.5)	33,755.8 (2.5)	8623.25				6.83×10^{-3}	3.86×10^{-3}	2.91×10^{-1}	2.53×10^{-1}	9400	−0.85
15,295.1 (4.5)	26,807.1 (5.5)	8686.64	15,404.86	26,707.79	8847.263	9.34×10^{-3}	6.40×10^{-3}	4.13×10^{-1}	4.04×10^{-1}	9330	−0.45
28,265.1 (3.5)	39,716.6 (3.5)	8732.30				2.87×10^{-4}	1.59×10^{-4}	1.30×10^{-2}	1.16×10^{-2}	9600	−0.08
22,159.1 (2.5)	33,598.6 (0.5)	8741.55				1.41×10^{-4}	1.74×10^{-5}	6.43×10^{-3}	9.12×10^{-4}	8990	−0.13
27,798.8 (4.5)	39,201.1 (2.5)	8769.91	27,766.82			4.24×10^{-3}	6.24×10^{-4}	1.96×10^{-1}	4.29×10^{-2}	9490	−0.45
20,527.2 (3.5)	31,890.1 (1.5)	8800.42				3.81×10^{-4}	9.92×10^{-5}	1.80×10^{-2}	5.50×10^{-3}	9090	−0.37
22,533.3 (1.5)	33,755.8 (2.5)	8910.83				6.37×10^{-3}	7.86×10^{-3}	3.20×10^{-1}	5.78×10^{-1}	9620	−0.80
22,533.3 (1.5)	33,598.6 (0.5)	9037.21				5.88×10^{-4}	1.39×10^{-4}	3.17×10^{-2}	8.16×10^{-3}	9200	0.70
28,265.1 (3.5)	39,201.1 (2.5)	9143.89				3.57×10^{-3}	1.00×10^{-3}	2.04×10^{-1}	9.45×10^{-2}	10,110	−0.36
10,184.6 (5.5)	20,527.2 (3.5)	9668.33	10,171.79			4.85×10^{-5}	9.20×10^{-6}	3.66×10^{-3}	9.99×10^{-4}	10400	0.17
−32.0 (7.5)	10,184.6 (5.5)	9787.86	0.00	10,171.79	9831.111	3.22×10^{-4}	1.76×10^{-4}	2.58×10^{-2}	1.45×10^{-2}	9840	0.49
24,723.5 (4.5)	34,889.8 (2.5)	9836.13	24,736.00			3.04×10^{-4}	1.78×10^{-4}	2.50×10^{-2}	1.22×10^{-2}	9490	0.07
26,807.1 (5.5)	36,928.1 (4.5)	9880.38	26,707.79			8.18×10^{-4}	5.05×10^{-4}	6.88×10^{-2}	4.03×10^{-2}	9780	−0.15
18,470.4 (1.5)	28,265.1 (3.5)	10,209.9				4.18×10^{-4}	1.25×10^{-3}	4.14×10^{-2}	1.56×10^{-1}	10,700	−0.68
12,399.5 (4.5)	22,159.1 (2.5)	10,245.8	12,468.66			1.06×10^{-4}	2.17×10^{-5}	1.07×10^{-2}	2.53×10^{-3}	10,550	0.26

Table 5. *Cont.*

Transition [a]						gA (s^{-1})		Line Strength S (a.u.)		Wavelength (Å)	CF
E_{Low_Fit} (cm^{-1})	E_{Upp_Fit} (cm^{-1})	λ_{Ritz_Fit} (Å)	E_{Low_Exp} (cm^{-1})	E_{Upp_Exp} (cm^{-1})	λ_{Ritz_Exp} (Å)	This Work	D&Z [19]	This Work	D&Z [19]	$\lambda_{D\&Z}$ [19]	This Work
22,159.1 (2.5)	31,890.1 (1.5)	10,276.3				1.51×10^{-4}	5.36×10^{-5}	1.55×10^{-2}	7.06×10^{-3}	10,810	0.09
24,723.5 (4.5)	34,405.9 (3.5)	10,327.9	24,736.00			8.71×10^{-4}	3.50×10^{-4}	9.14×10^{-2}	4.99×10^{-2}	10,980	0.18
15,295.1 (4.5)	24,723.5 (4.5)	10,606.3	15,404.86	24,736.00	10,716.80	4.80×10^{-5}	2.29×10^{-5}	5.75×10^{-3}	3.31×10^{-3}	11,010	0.02
22,533.3 (1.5)	31,890.1 (1.5)	10,687.4				9.10×10^{-5}	7.84×10^{-5}	1.13×10^{-2}	1.18×10^{-2}	11,110	0.08
10,184.6 (5.5)	19,385.4 (5.5)	10,868.4	10,171.79	19,331.69	10,917.15	2.46×10^{-4}	1.37×10^{-4}	3.34×10^{-2}	2.94×10^{-2}	11,920	0.71
27,798.8 (4.5)	36,928.1 (4.5)	10,953.7	27,766.82			1.19×10^{-5}	3.31×10^{-5}	1.68×10^{-3}	4.28×10^{-3}	10,770	−0.02
24,723.5 (4.5)	33,755.8 (2.5)	11,071.3	24,736.00			1.64×10^{-4}	3.20×10^{-5}	2.44×10^{-2}	7.03×10^{-3}	11,970	0.07
19,385.4 (5.5)	28,265.1 (3.5)	11,261.5	19,331.69			7.46×10^{-6}	2.14×10^{-6}	1.21×10^{-3}	4.34×10^{-4}	11,790	0.00
24,723.5 (4.5)	33,577.5 (6.5)	11,295.1	24,736.00			1.47×10^{-4}	2.07×10^{-4}	2.41×10^{-2}	3.55×10^{-2}	11,390	0.04
19,385.4 (5.5)	28,232.5 (7.5)	11,303.9	19,331.69			5.95×10^{-4}	6.22×10^{-4}	9.80×10^{-2}	1.08×10^{-1}	11,420	−0.15
6533.4 (6.5)	15,295.1 (4.5)	11,412.7	6507.750	15,404.86	11,239.60	5.29×10^{-5}	1.76×10^{-5}	9.15×10^{-3}	4.26×10^{-3}	12,210	−0.54
28,265.1 (3.5)	36,928.1 (4.5)	11,543.4				4.01×10^{-5}	3.42×10^{-5}	7.33×10^{-3}	6.33×10^{-3}	11,570	0.01
19,385.4 (5.5)	27,798.8 (4.5)	11,885.7	19,331.69	27,766.82	11,855.18	9.70×10^{-5}	3.97×10^{-5}	2.05×10^{-2}	1.20×10^{-2}	12,760	−0.45
12,399.5 (4.5)	20,527.2 (3.5)	12,303.0	12,468.66			5.87×10^{-5}	3.14×10^{-5}	1.48×10^{-2}	1.02×10^{-2}	12,940	−0.15
31,890.1 (1.5)	39,716.6 (3.5)	12,777.2				1.39×10^{-4}	2.47×10^{-4}	4.22×10^{-2}	1.66×10^{-1}	14,980	0.23
20,527.2 (3.5)	28,265.1 (3.5)	12,923.6				3.58×10^{-4}	2.27×10^{-4}	1.15×10^{-1}	1.01×10^{-1}	13,780	−0.28
26,807.1 (5.5)	34,405.9 (3.5)	13,159.7				6.08×10^{-6}	3.53×10^{-6}	2.14×10^{-3}	1.36×10^{-3}	13,390	0.02
19,385.4 (5.5)	26,807.1 (5.5)	13,473.9	19,331.69	26,707.79	13,557.30	1.08×10^{-6}	2.17×10^{-7}	4.27×10^{-4}	1.25×10^{-4}	14,510	−0.02
31,890.1 (1.5)	39,201.1 (2.5)	13,678.1				1.83×10^{-4}	1.37×10^{-4}	7.83×10^{-2}	1.39×10^{-1}	16,270	0.47
20,527.2 (3.5)	27,798.8 (4.5)	13,752.4		27,766.82		1.31×10^{-3}	1.03×10^{-3}	5.75×10^{-1}	7.27×10^{-1}	15,120	−0.82
27,798.8 (4.5)	34,889.8 (2.5)	14,101.8	27,766.82			4.01×10^{-4}	2.62×10^{-4}	2.00×10^{-1}	7.32×10^{-2}	12,560	0.78
12,399.5 (4.5)	19,385.4 (5.5)	14,314.2	12,468.66	19,331.69	14,570.82	3.52×10^{-4}	4.10×10^{-4}	1.89×10^{-1}	3.14×10^{-1}	15,370	−0.64
15,295.1 (4.5)	22,159.1 (2.5)	14,568.3	15,404.86			8.85×10^{-7}	4.33×10^{-8}	5.19×10^{-4}	2.67×10^{-5}	14,720	0.01
26,807.1 (5.5)	33,577.5 (6.5)	14,771.3	26,707.79			3.59×10^{-5}	6.13×10^{-5}	2.25×10^{-2}	2.93×10^{-2}	13,990	0.36
28,265.1 (3.5)	34,889.8 (2.5)	15,094.5				6.30×10^{-5}	7.80×10^{-5}	4.41×10^{-2}	3.32×10^{-2}	13,670	0.09
27,798.8 (4.5)	34,405.9 (3.5)	15,134.9	27,766.82			7.99×10^{-7}	6.55×10^{-7}	5.66×10^{-4}	4.95×10^{-4}	15,330	0.00
−32.0 (7.5)	6533.4 (6.5)	15,231.3	0.00	6507.750	15,366.29	2.50×10^{-5}	1.62×10^{-5}	1.83×10^{-2}	1.21×10^{-2}	15,280	0.93
27,798.8 (4.5)	33,577.5 (6.5)	17,306.6	27,766.82			7.54×10^{-6}	8.89×10^{-6}	1.04×10^{-2}	8.64×10^{-3}	16,120	−0.05

[a] λ_{Ritz_Fit} (col. 3) and λ_{Ritz_Exp} (col. 6) are respectively calculated from least-squares fitted energies (col. 1 and 2) and experimental energies (col. 4 and 5) in [14].

It is worth examining the particular case of the M1 line at 1.5 μm, which is widely used for fiber amplifiers in optical communication. The Ritz wavelength derived from the experimental energies of the ground state $4f^{11}\,{}^4I_{15/2}$ and the first excited state $4f^{11}\,{}^4I_{13/2}$ [14] is λ_{Ritz_Exp} = 15,366.3 Å, and it should be the best wavelength prediction for the free ion. As for the transition probabilities, our semi-empirical prediction is λ_{Ritz_Fit} = 15,231.3 Å, gA = 144.4 s^{-1} and S = 18.92 a.u., whereas the ab initio calculations report $\lambda_{D\&Z}$ = 15,280 Å, gA = 142.8 s^{-1} and S = 18.89 a.u. The relative discrepancy on gA is $\Delta(gA)/gA = 1.1 \times 10^{-2}$ and only $\Delta S/S = 1.6 \times 10^{-3}$ on line strength. It means that uncertainties on wavelengths propagate into gA values. A scaling of calculated values of gA with a factor $(\lambda_{calc.}/\lambda_{Ritz\_exp})^3$ or $(\lambda_{calc.}/\lambda_{Ritz\_exp})^5$ could lead to an improvement in applications. Emission in aqueous solution was predicted [3] at 15,129 Å, with a magnetic dipole oscillator strength of 30.82×10^{-8}, i.e., gA = 143.7 s^{-1} and S = 18.45 a.u.

3.4. Scaling Factors of Energy Parameters as Derived from Least-Squares Fits

As explained in our previous parametric studies, in order to obtain a meaningful least-squares fit of the energy parameters and consequently reliable energy predictions, we strived to reduce the number of free parameters by applying constraints on some parameters, either by fixing their values or by fixing their ratios to their HFR values. The choice of good initial values of the parameters is therefore important. Table 6 shows a comparison of scaling factors among several neighboring spectra of lanthanide ions. The first four columns were already discussed in [25], and the more recent results on Yb V and Er IV confirm the consistency of these scaling factors, which helps for the choice of their initial values, including the effective parameters that are used for taking interactions with far unknown configurations into account.

Table 6. Consistency of scaling factor (SF) values of energy parameters $SF = P_{fit}/P_{HFR}$ among neighboring spectra of lanthanide ions. An example of effective CI parameter F^1(4f,5d) values is given.

	Scaling Factor					
Parameters	**Nd IV [7]**	**Nd V [9]**	**Tm IV [10]**	**Er II [21]**	**Yb V [11]**	**Er IV [14]**
	$4f^3$+ ...	**$4f^2$ + 4f6p**	**$4f^{12}$ + $4f^{11}$6p**	**$4f^{12}$6p**	**$4f^{12}$ + $4f^{11}$6p**	**$4f^{11}$ + $4f^{10}$6p**
	$4f^2$5d+ ...	**4f5d+ ...**	**$4f^{11}$5d+ ...**	**$4f^{12}$5d ...**	**$4f^{11}$5d+ ...**	**$4f^{10}$5d+ ...**
F^2(4f,4f)	0.768	0.761	0.785	0.763	0.800	0.779
F^4(4f,4f)	0.839	0.852	0.868	0.844	0.898	0.880
F^6(4f,4f)	0.797	0.766	0.855	0.930	0.864	0.877
ζ_{4f}	0.932	0.927	0.982	0.981	0.982	0.991
F^2(4f,5d)	0.758	0.763	0.806	0.816	0.807	0.804
F^4(4f,5d)	1.082	1.100	1.132	1.174	1.129	1.152
G^1(4f,5d)	0.846	0.860	0.751	0.683	0.774	0.693
G^3(4f,5d)	0.954	0.983	0.974	1.013	0.960	0.966
G^5(4f,5d)	0.839	0.868	0.830	0.753	0.843	0.822
F^2(4f,6p)	0.797	0.815	0.867	0.820	0.844	0.803
ζ_{6p}	1.207	1.168	1.17	1.320	1.143	1.173
F^1(4f,5d) (cm^{-1})	758 ± 57	839 ± 147	866 ± 106	902 ± 62	819 ± 81	1066 ± 109

4. Conclusions

We have shown that it is possible to perform rather simple calculations using Cowan codes [15] to obtain reliable transition probabilities for forbidden transitions such as magnetic dipole (M1) and electric quadrupole transitions (E2) within the ground-state configurations of the lanthanide ions, provided that experimental level energies are known and good parametric studies can be carried out. The good agreement between our results and the results of existing ab initio and semi-empirical calculations in Tm IV and Yb V allow for confidence in the first parametric calculations for Er IV. Generally speaking, agreements between different calculations are more satisfactory for the magnetic

dipole transitions than for the electric quadrupole transitions. In the absence of experimental data for a systematic investigation of the reliability of calculations, the cancellation factor, as defined by Cowan [15], is the only possible criterion. A good correlation between observed intensities and the computed gf values for CF that are greater than about 0.02, was found in the case of Dy I as quoted by Cowan [15]. Furthermore, in a discussion about oscillator strength determination for rare-earth elements and ions, Biémont set the limit to 0.01, under which the transition may be affected by severe cancellation effects [26]. Being aware that these considerations are based on the observed intensities of allowed electric dipole transitions, one may apply with caution the criterion of $|CF| > 0.01$ or 0.02 to forbidden transitions. Unfortunately, for the last, meaningful conclusions can be drawn only if systematic comparison of observed intensities and calculated transition probabilities becomes possible.

Author Contributions: All authors had equal contribution.

Funding: Financial support of the French CNRS–Stellar Physics National Program (PNPS) is acknowledged. This work is part of the Plas@Par LabEx project managed by the ANR (ANR-11-IDEX-0004-02). A.M. and S.A.M. wish to acknowledge supports from University Mouloud Mammeri, Tizi-Ouzou, Algeria, and from the project CNEPRU D00520110032, Algeria.

Acknowledgments: The authors are grateful to A. Kramida for maintaining the Windows version of the Cowan codes and for helpful answers about their operations. WULTB wishes to thank T. Brage and R. Hutton for useful discussions at the ExTra workshop in Fudan University.

Conflicts of Interest: The authors declare no conflict of interest.

References

1. Wybourne, B.G. The fascination of the rare earths—Then, now and in the future. *J. Alloys Compd.* **2004**, *380*, 96–100. [CrossRef]
2. Carnall, W.T.; Fields, P.R.; Wybourne, B.G. Spectral intensities of the trivalent lanthanides and actinides in solution. I. Pr^{3+}, Nd^{3+}, Er^{3+}, Tm^{3+}, and Yb^{3+}. *J. Chem. Phys.* **1965**, *42*, 3797–3806. [CrossRef]
3. Carnall, W.T.; Fields, P.R.; Wybourne, B.G. Spectral intensities of the trivalent lanthanides and actinides in solution. II. Pm^{3+}, Sm^{3+}, Eu^{3+}, Gd^{3+}, Tb^{3+}, Dy^{3+}, and Ho^{3+}. *J. Chem. Phys.* **1968**, *49*, 4412–4423. [CrossRef]
4. Ryabchikova, T.; Ryabtsev, A.N.; Kochukov, O.; Bagnulo, S. Rare-earth elements in the atmosphere of the magnetic chemically peculiar star HD 144897. New classification of the Nd III spectrum. *Astron. Astrophys.* **2006**, *456*, 329–338. [CrossRef]
5. Kasen, D.; Badnell, N.R.; Barnes, J. Opacities and spectra of the r-process ejecta from neutron star mergers. *Astrophys. J.* **2013**, *774*, 25. [CrossRef]
6. Fontes, C.J.; Fryer, C.L.; Hungerford, A.L.; Hakel, P.; Colgan, J.; Kilcrease, D.P.; Sherrill, M.E. Relativistic opacities for astrophysical applications. *High Energy Density Phys.* **2015**, *16*, 53–59. [CrossRef]
7. Wyart, J.-F.; Meftah, A.; Bachelier, A.; Sinzelle, J.; Tchang-Brillet, W.-Ü.L.; Champion, N.; Spector, N.; Sugar, J. Energy levels of $4f^3$ in the Nd^{3+} free ion from emission spectra. *J. Phys. B Mol. Opt. Phys.* **2006**, *39*, L77. [CrossRef]
8. Wyart, J.-F.; Meftah, A.; Tchang-Brillet, W.-Ü.L.; Champion, N.; Lamrous, O.; Spector, N.; Sugar, J. Analysis of the free ion Nd^{3+} spectrum (Nd IV). *J. Phys. B At. Mol. Opt. Phys.* **2007**, *40*, 3957–3972. [CrossRef]
9. Wyart, J.-F.; Meftah, A.; Sinzelle, J.; Tchang-Brillet, W.-Ü.L.; Spector, N.; Judd, B. Theoretical study of ground-state configurations $4f^N$ in Nd IV, Pr IV and Nd V. *J. Phys. B At. Mol. Opt. Phys.* **2008**, *41*, 085001. [CrossRef]
10. Wyart, J.-F.; Meftah, A.; Sinzelle, J.; Tchang-Brillet, W.-Ü.L.; Champion, N.; Spector, N.; Sugar, J. Spectrum and energy levels of the Nd^{4+} free ion (Nd V). *Phys. Scr.* **2008**, *77*, 055302.
11. Meftah, A.; Wyart, J.-F.; Champion, N.; Tchang-Brillet, W.-Ü.L. Observation and interpretation of the Tm^{3+} free ion spectrum. *Eur. Phys. J. D* **2007**, *44*, 35–45. [CrossRef]
12. Meftah, A.; Wyart, J.-F.; Tchang-Brillet, W.-Ü.L.; Blaess, C.; Champion, N. Spectrum and energy levels of the Yb^{4+} free ion (Yb V). *Phys. Scr.* **2013**, *88*, 045305. [CrossRef]
13. Deghiche, D.; Meftah, A.; Wyart, J.-F.; Champion, N.; Blaess, C.; Tchang-Brillet, W.-Ü.L. Observation of core-excited configuration in four-time ionized neodymium Nd^{4+} (Nd V). *Phys. Scr.* **2015**, *90*, 095402. [CrossRef]

14. Meftah, A.; Ait Mammar, S.; Wyart, J.-F.; Tchang-Brillet, W.-Ü.L.; Champion, N.; Blaess, C.; Deghiche, D.; Lamrous, O. Analysis of the free ion spectrum of Er^{3+} (Er IV). *J. Phys. B At. Mol. Opt. Phys.* **2016**, *49*, 165002. [CrossRef]
15. Cowan, R.D. *The Theory of Atomic Structure and Spectra*; University of California Press: Berkeley, CA, USA, 1981.
16. Kramida, A. A Suite of Atomic Structure Codes Originally Developed by R. D. Cowan Adapted for Windows-Based Personal Computers. Available online: http://das101.isan.troitsk.ru/COWAN (accessed on 5 May 2017).
17. Judd, B.R. Optical absorption intensities of rare-earth ions. *Phys. Rev.* **1962**, *127*, 750–761. [CrossRef]
18. Ofelt, G.S. Intensities of crystal spectra of rare-earth ions. *J. Chem. Phys.* **1962**, *37*, 511–520. [CrossRef]
19. Dodson, C.M.; Zia, R. Magnetic dipole and electric quadrupole transitions in the trivalent lanthanide series: Calculated emission rates and oscillator strengths. *Phys. Rev. B* **2012**, *86*, 126102. [CrossRef]
20. Enzonga Yoca, S.; Quinet, P. Radiative decay rates for electric dipole, magnetic dipole and electric quadrupole transitions in triply ionized Thulium (Tm IV). *Atoms* **2017**, *5*, 28. [CrossRef]
21. Li, H.; Kuang, X.-Y.; Yeung, Y.Y. Semi-empirical calculations of radiative rates for parity-forbidden transitions within the $4f^2$ configuration of Ba-like ions La^+, Ce^{2+}, Pr^{3+} and Nd^{4+} and $4f^{12}$ configuration of Dy-like Yb^{4+}. *J. Phys. B At. Mol. Opt. Phys.* **2014**, *47*, 145002. [CrossRef]
22. Kramida, A.E. The program LOPT for least-squares optimization of energy levels. *Comput. Phys. Commun.* **2010**, *182*, 419–434. [CrossRef]
23. Kramida, A.; Ralchenko, Y.; Reader, J. *NIST ASD Team. NIST Atomic Spectra Database*; version 5.5.6; National Institute of Standards and Technology: Gaithersburg, MD, USA, 2018. Available online: https://physics.nist.gov/asd (accessed on 7 August 2018).
24. Meftah, A. (Observatoire de Paris-Meudon, PSL Research University, Meudon, France and Université Mouloud Mammeri, Tizi-Ouzou, Algeria). Personal communication, 2017.
25. Wyart, J.-F. On the interpretation of complex atomic spectra by means of the parametric Racah-Slater method and Cowan codes. *Can. J. Phys.* **2011**, *89*, 451–456. [CrossRef]
26. Biémont, E. Recent advances and difficulties in oscillator strength determination for rare-earth elements and ions. *Phys. Scr.* **2005**, *T119*, 55–60. [CrossRef]